Available online at www.sciencedirect.com
SCIENCE DIRECT®
Scripta Materialia 53 (2005) 395–401
Scripta MATERIALIA
www.actamat-journals.com

Magnetization reversal process in FePt $L1_0$ nanoparticles

S. Okamoto [a,*], N. Kikuchi [b], O. Kitakami [a], Y. Shimada [a]

[a] *Institute of Multidisciplinary Research for Advanced Materials, Tohoku University, Katahira 2-1-1, Aoba-Ku, Sendai 980-8577, Japan*
[b] *MESA+ Research Institute, SMI, University of Twente, 7500 AE, Enschede, The Netherlands*

Received 13 October 2004; received in revised form 29 December 2004; accepted 21 April 2005
Available online 23 May 2005

Abstract

We have studied the magnetization reversals of FePt $L1_0$ particles. Lithographically fabricated single FePt particles and well isolated epitaxial FePt $L1_0$ nanoparticles have been investigated for a wide range of particle diameters D. Careful analyses of the experiments have revealed that for particles larger than 20 nm the magnetization reversal behaviors are governed by either nucleation or expansion of a reversed domain depending on the temperature, and the coherent rotation mode becomes dominant for $D < 20$ nm.
© 2005 Acta Materialia Inc. Published by Elsevier Ltd. All rights reserved.

Keywords: Iron alloys; Platinum-group; Magnetic thin films; Magnetic anisotropy; Magnetic recording

1. Introduction

Magnetic recording has been a key technology for high-density information storage, and recording density has been increasing at a tremendous rate. This has been achieved by reducing not only the magnetic particle size but also the number of magnetic particles in one bit. For a recording density more than 1 Terabit/in.^{2}, one bit is expected to contain a few particles [1]. On the other hand, for patterned media and newly emerging spintronic storage devices, such as magnetic random access memory, one magnetic element is used as a memory cell unit. Therefore, deeper understanding of the reversal process of a nanomagnet is required.

Magnetization reversal problems, such as Brown's paradox [2] and the coercivity mechanism in a hard magnet [3,4], have been discussed for a very long time. However, there are many experimental difficulties in clarifying these problems. For instance, magnetic specimens usually consist of a great number of crystallites with structural (size, crystal orientation, etc.) and/or magnetic inhomogeneities.

In this study, we have investigated the magnetization reversal process of FePt $L1_0$ particles. FePt $L1_0$ is one of the prominent candidates for future ultra-high density recording media because of its very high magnetic anisotropy [5]. In addition to such technological importance, the high magnetic anisotropy of FePt can suppress thermal agitation of spins even at the nanoscale. This is a great advantage for the study of magnetization reversal in a nanomagnet. This paper consists of the following two topics. The first is a lithographically fabricated single FePt $L1_0$ particle [6,7], whose reversal process has been measured by means of the anomalous Hall effect (AHE). The second is epitaxially grown FePt $L1_0$ (0 0 1) nanoparticles [7,8]. Such well isolated single crystal nanoparticles enable us to study magnetic behaviors in the size range much smaller than the resolution limit of our e-beam lithography.

2. Lithographically fabricated single FePt $L1_0$ particle

A single FePt $L1_0$ particle was patterned from a (0 0 1) single crystal film. First, a 10 nm thick FePt film was

* Corresponding author. Tel.: +81 222 175 359; fax: +81 222 175 404.
E-mail address: okamoto@tagen.tohoku.ac.jp (S. Okamoto).

1359-6462/$ - see front matter © 2005 Acta Materialia Inc. Published by Elsevier Ltd. All rights reserved.
doi:10.1016/j.scriptamat.2005.04.034

epitaxially grown on a MgO(100) single crystal substrate by dc magnetron sputtering. Substrate temperature was fixed at 973 K. A highly ordered $L1_0$ phase was obtained and its crystalline orientation was (001) without any crystal domain variants [5]. The degree of $L1_0$ ordering was about 0.6. The temperature dependence of the effective anisotropy field H_k^{eff} including the demagnetizing field, which is determined by the generalized Sucksmith–Thompson (GST) method [5]. In this method, H_k^{eff} can be accurately evaluated by analyzing vector magnetization behavior under various tilted magnetic fields. The result is about 40 kOe and remains almost constant in the temperature range from 10 to 300 K. The vertical magnetization curve measured by the magneto optical Kerr effect is square shape. The coercivity H_c is about 3 kOe, which is almost one order of magnitude smaller than H_k^{eff}, suggesting that the magnetization reversal proceeds through nucleation and subsequent expansion of reversed domain. The domain structure of demagnetized film observed by the magnetic force microscopy (MFM) is stripe pattern with 200–300 nm width.

This FePt single crystal film was patterned into a disk shaped particle by using electron beam (EB) lithography and ion beam etching. The minimum size in our lithographic technique was $D = 60$ nm. The 5 nm Pt overlayer was subsequently deposited on the FePt particle and then patterned into a cross shaped electrode for AHE measurements [6]. Fig. 1 shows an example of a scanning electron microscope (SEM) image for a single FePt particle covered with a Pt electrode. The measurement sensitivity is mainly determined by the AHE amplitude of FePt and the shunt effect between the particle and the electrode, which depends on the size and material of the electrode. To reduce the shunt effect, the electrode width should be sufficiently narrow. According to our finite element calculations and preliminary experiments [6], the AHE signal from a FePt nanoparticle can be detected even when the Pt electrode width is 10 times larger than the particle diameter due to the very large AHE coefficient of FePt, which is about 100 times larger than that of Co [9].

Vertical magnetization loops for a single FePt particle with $D = 60$–700 nm are shown in Fig. 2. All the curves are perfectly square. Initial magnetization curves indicated by white circles were measured after applying the in-plane magnetic field of 70 kOe, which is sufficiently larger than H_k^{eff}. Note that the initial and major magnetization curves for $D = 60$ nm coincide each other, indicating that a bi-stable single domain state is realized. On the other hand, the initial curve obviously deviates from the major one for $D \geqslant 80$ nm, suggesting that the initial demagnetized state is a multidomain state. Therefore, it is concluded that the critical size between single and multidomain states is $D = 60$–80 nm. This value is much smaller than the domain width of 200–300 nm for the unpatterned film. For $D \geqslant 80$ nm, the FePt particle metastably goes into the single domain state once it is saturated, because the saturation field of the initial curve is much smaller than the reversal field of the major magnetization curve.

The reversal fields H_r of these single particles are about 6–8 kOe and almost insensitive to the particle size. These values are somewhat larger than that of the unpatterned film but still much smaller than H_k^{eff}. Fig. 3 shows the angular dependence of H_r for $D = 200$ nm. The abscissa is the field angle θ_H from the sample normal. Although H_r values at 10 and 300 K are much different, their angular dependences are quite similar and seem to follow the function of $1/\cos\theta_H$. Similar results

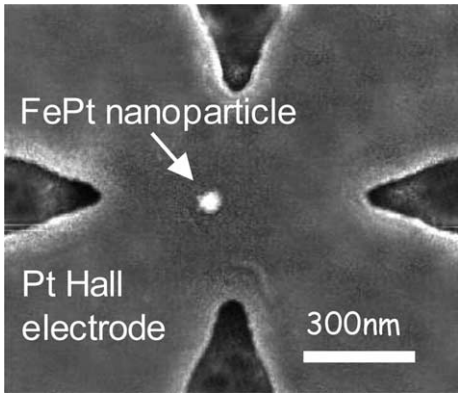


Fig. 1. SEM image of a lithographically fabricated FePt $L1_0$ nanoparticle with 60 nm in diameter embedded in a Pt cross-shaped electrode [7].

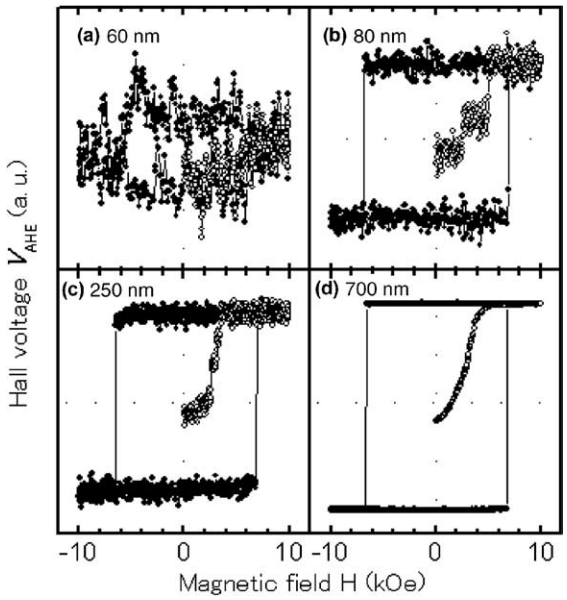


Fig. 2. AHE curves at 300 K for single FePt particles with $D = 60$, 80, 250, and 700 nm in diameter. The open and solid circles represent the initial and full magnetization curves, respectively [7].

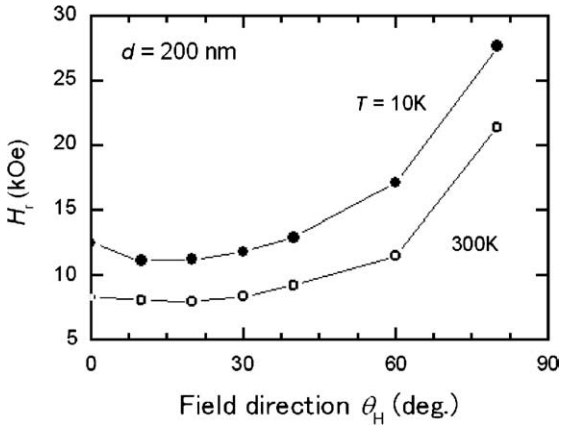


Fig. 3. Reversal field H_r for a single FePt particle with $D = 200$ nm as a function of magnetic field direction θ_H from the sample normal [7].

were also obtained for $D = 60$ nm. These $1/\cos\theta_H$ type behaviors suggest that the magnetization reversal proceeds through nucleation and displacement of reversed domains.

In order to investigate the influence of thermal agitation on the magnetization reversal in a FePt single particle, we have evaluated reversal probability $p(H)$ as a function of the field by repeating magnetic loop measurements many times for one FePt particle at a fixed temperature. An example for particle with $D = 160$ nm measured at 300 K is shown in Fig. 4, where the horizontal axis indicates the field at which the reversal events occur. In the present study, we have repeated the measurements 12 times at each temperature. In spite of measurements for the same particles ($D = 160$ nm), the reversal fields H_r distribute in the range of $H_r = 8.01$–8.16 kOe due to the thermal agitation effect. Here, average reversal field H_r^{av} and reversal field distribution ΔH_r are, respectively, defined as the field at $p(H) = 0.5$ and field interval between $p(H) = 0.3$ and 0.7. Their temperature dependences are shown in Fig. 5(a) and (b). It is

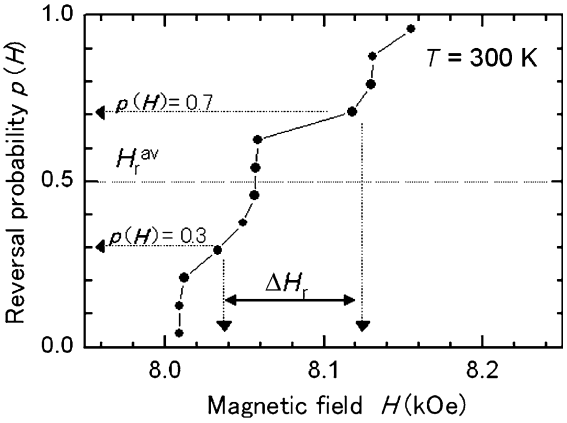


Fig. 4. Reversal provability $p(H)$ at 300 K for a single FePt particle with $D = 160$ nm as a function of applied field [7].

clearly mentioned that H_r^{av} decreases monotonically with temperature and shows a distinct deflection at $T \sim 150$ K. Since H_k^{eff} is almost constant in this temperature range as mentioned above, this decrease of H_r^{av} is attributed to the influence of thermal agitation. Around the deflection point ($T \sim 150$ K) in Fig. 5(a), ΔH_r in Fig. 5(b) shows large scattering.

Let us discuss the above temperature dependences of H_r^{av} and ΔH_r. As mentioned above, the magnetization reversal in our samples proceed through nucleation and subsequent expansion of a reversed domain. According to the classical bubble domain theory [10], there is a critical size δ_c for expansion of a reversed domain, at which total magnetic energy $E_{total} = E_z + E_w + E_d$ takes a maximum, where E_z is Zeeman energy, E_w the wall energy, and E_d the demagnetizing energy. Although analytic calculation of δ_c is very complicated, variation of δ_c against the reverse field can be roughly estimated as shown schematically by the solid line in Fig. 6, because E_z is the expansion term in proportion to the volume of a reversed domain and E_w is the contraction term in proportion to the wall area surrounding a domain. Our numerical calculation gave $\delta_c \sim 8$ nm at $H = 10$ kOe for FePt particle ($M_s = 1100$ emu/cc, exchange stiffness $A = 1 \times 10^{-6}$ erg/cm, $K_u = 3 \times 10^{-7}$

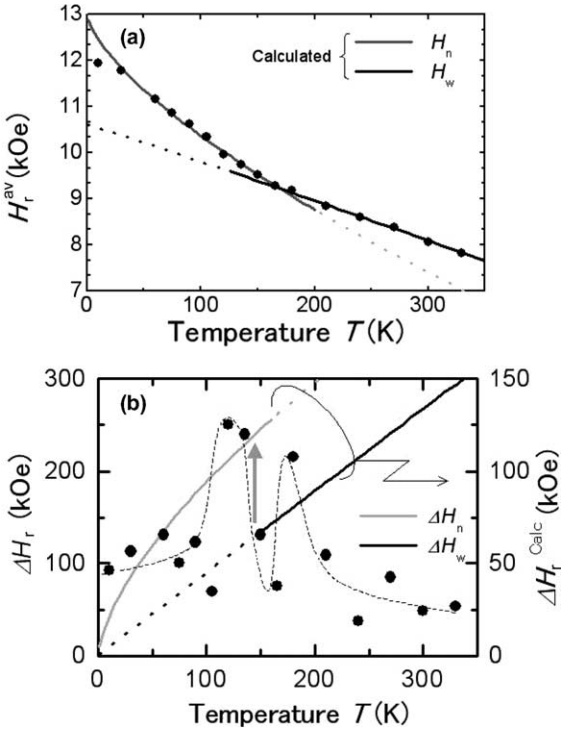


Fig. 5. Temperature dependence of (a) average reversal field H_r^{av} and (b) its dispersion ΔH_r for a single FePt particle with $D = 160$ nm. The gray and black lines in (a), respectively, indicate the best fittings of fields H_n and H_w for nucleation- and expansion-type reversal modes in Eq. (2). The gray and black lines in (b) are the calculated ΔH_r using the best fitting results in (a). The arrow in (b) suggests the discontinuous change in the calculated ΔH_r [7].

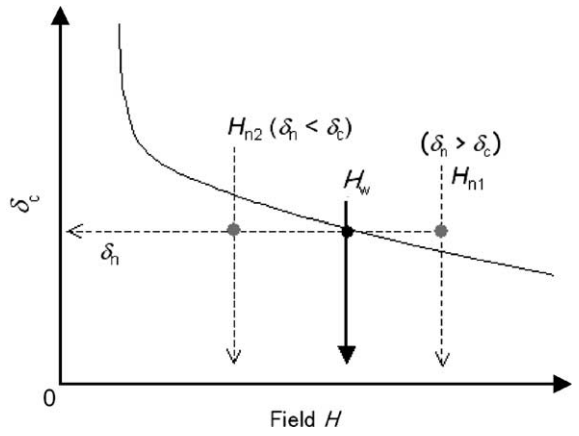


Fig. 6. Schematic of critical size δ_c for expansion of a reversed embryo as a function of applied field [7].

erg/cc). At the very beginning of the magnetization reversal, a reversed embryo with the size of δ_n would nucleate when a reverse field reaches a certain nucleation field H_n. If $\delta_n \geqslant \delta_c$ at $H = H_{n1}$ as shown in Fig. 6, the embryo will spontaneously expand over the entire particle. In this case, the magnetization reversal is exclusively governed by the nucleation event. As the temperature increases, however, the nucleation event will be assisted by thermal energy, resulting in the reduction of the nucleation field, such as from H_{n1} to H_{n2} in Fig. 6. Since $\delta_n < \delta_c$ at $H = H_{n2}$, the reversed embryo cannot expand until it becomes δ_c by further increase in the reverse field. Therefore, in this case, the reversal process is dominated by expansion or displacement of a reversed embryo. As mentioned above, it is expected that the reversal process depends on the temperature; nucleation of a reversed embryo governs the reversal events at lower temperature, while its expansion or displacement becomes dominant at higher temperature.

Based on the above discussion, the experimental results in Fig. 5(a) and (b) are analyzed as follows. The energy barrier for nucleation or expansion of a reversed embryo is a function of H and can be expressed as [11]

$$E_i(H) = E_{i0}[1 - H/H_{i0}]^{\alpha_i}, \quad (i = \mathrm{n}, \mathrm{w}), \tag{1}$$

where $E_{n0\,(w0)}$ denotes the energy barrier at zero field for nucleation (expansion) of a reversed embryo, $H_{n0\,(w0)}$ the intrinsic critical field for nucleation (expansion) of a reversed embryo without thermal activation, and $\alpha_{n\,(w)} = 1.5$ (1) the scaling exponent depending on reversal modes [11]. For simplicity, $E_{n0\,(w0)}$ and $H_{n0\,(w0)}$, which may be functions of temperature, are treated as constants. By adopting the Néel–Arrhenius type relaxation [12], the probability for nucleation (expansion) of a reversed embryo can be expressed as [13]

$$p_i(H) = 1 - \exp\left[-f_0/R \int_0^H \exp\{-E_i(H')/k_B T\}\,\mathrm{d}H'\right] \quad (i = \mathrm{n}, \mathrm{w}), \tag{2}$$

where $f_0 = 10^{10}\ \mathrm{s}^{-1}$ is the attempt frequency, R the field sweep rate, and k_B Boltzmann constant. The solid lines in Fig. 5(a) are the best fitting results of Eq. (2) assuming the nucleation type for $T < 150$ K and the expansion type for $T > 150$ K. As can be seen in this figure, the deflection of the slope at $T \sim 150$ K can be reproduced very well, and thus obtained parameters are $E_{n0} = 3.4 \times 10^{-12}$ erg and $H_{n0} = 13$ kOe for the nucleation type and $E_{w0} = 4.0 \times 10^{-12}$ erg and $H_{w0} = 11$ kOe for the expansion type, respectively. We also measured the sweep rate dependence of the reversal field at $T = 280$–315 K, and obtained $E_{w0} = 3.8 \times 10^{-12}$ erg and $H_{w0} = 11$ kOe by analyzing the data using Eq. (2) [13]. These values are in good agreement with those evaluated from temperature dependence of H_r. If the critical size of reversed embryo is nearly equal to its exchange length as proposed by Givord [3], the energy barrier is estimated to be $\gamma_w l_{ex}^2 \sim 7 \times 10^{-12}$ erg, where $\gamma_w = 4\sqrt{AK_u}$ is the wall energy and $l_{ex} = \pi\sqrt{A/K_u}$ the exchange length. This estimation is in good agreement with the above fitting results. Furthermore, the exchange length of our FePt particle is evaluated to be about 6 nm, which is almost equal to the critical size numerically calculated from the bubble domain theory as mentioned above. Thus determined fitting parameters enable us to calculate the reversal field distribution ΔH_r, as indicated by the gray and black solid lines in Fig. 5(b), and discontinuous change in the calculated ΔH_r appears where the reversal mode changes at $T \sim 150$ K. As a result, significant scattering in the data of ΔH_r at $T \sim 150$ K would be attributed to the change in the reversal modes, although there still remain some discrepancies, such as the values of ΔH_r and the behavior for $T > 200$ K.

3. Epitaxially grown FePt $L1_0$ nanoparticles

In this section, we will discuss the magnetization reversals of FePt $L1_0$ nanoparticles in the size range below the resolution limit of our EB lithography. The samples used here are single crystal FePt nanoparticles deposited on MgO(1 0 0) single crystal substrates at high temperature [8]. Since the nominal deposition thickness d was in the ultrathin thickness region from 3 to 0.5 nm, FePt is epitaxially grown in the form of an island nanoparticle. Depositions were carried out by dc magnetron sputtering at the substrate temperature of 973 K. Fig. 7 shows an example of an atomic force microscopy (AFM) image for $d = 1$ nm. Formation of FePt nanoparticles is clearly noticed. From the structural analyses, both the average diameter D and height h were almost proportional to d, that is, $D \sim 10d$, and $h \sim 2d$. Therefore, the particle shape is a thin oblate sphere with an aspect ratio of ~1/5. $L1_0$ ordering and (0 0 1) epitaxial growth were confirmed by the reflection

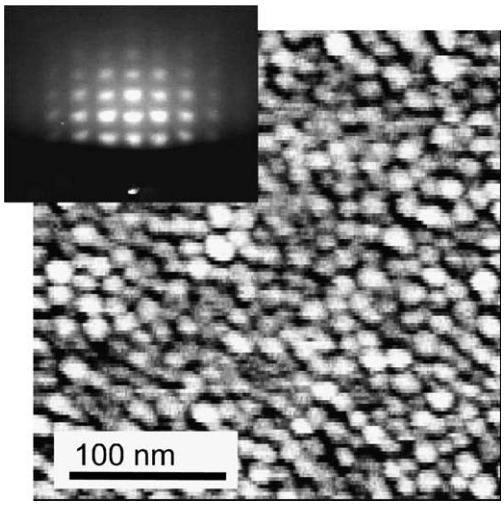


Fig. 7. AFM image of FePt $L1_0$ nanoparticle array epitaxially grown on MgO(100). The nominal deposition thickness d is 1 nm. The inset shows the RHEED image taken along MgO[110] [7].

high-energy electron diffraction (RHEED), as shown in the inset of Fig. 7.

Magnetization curves were measured by AHE measurements. A 4 nm Ag overlayer was deposited on the fully isolated FePt nanoparticles as an electrode for AHE measurement. Owing to the very high sensitivity of AHE measurement, hysteresis loops can be clearly detected even for a very thin FePt with $d = 0.5$ nm, as shown in Fig. 8. Temperature dependences of H_c determined from these AHE measurements are plotted in Fig. 9. Although H_c for smaller particles significantly decreases with temperature due to thermal fluctuation, H_c for all samples converges to almost the same value of 60–70 kOe at low temperature. The angular dependence of the reversal field (remanent coercivity) H_r exhibits the asteroid type behavior for $d = 1$ nm ($D \sim 10$ nm, $h \sim 2$ nm), as shown in Fig. 10. This result indicates that these FePt particles behave in accordance

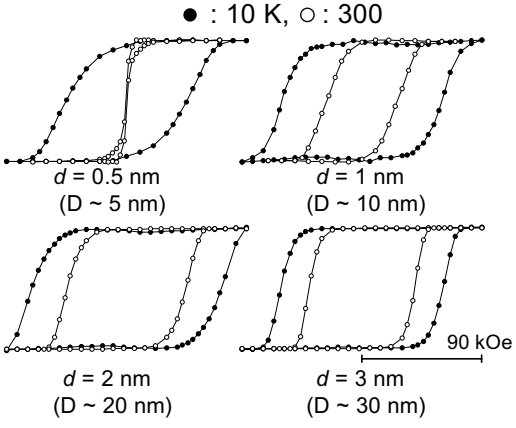


Fig. 8. AHE curves for epitaxially grown FePt $L1_0$ nanoparticle array with $d = 0.5$, 1, 2 and 3 nm [7].

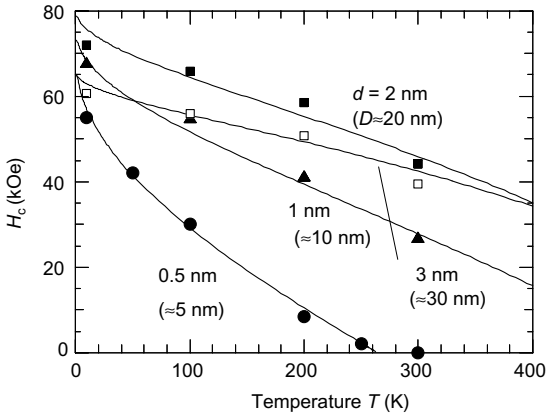


Fig. 9. Temperature dependences of H_c for epitaxially grown FePt $L1_0$ nanoparticle array. The solid lines indicate the best fitting using Eq. (3) [7].

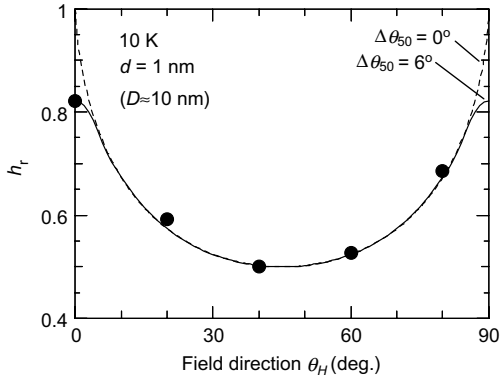


Fig. 10. Remanent coercivity H_r for epitaxially grown FePt $L1_0$ nanoparticle array with $d = 1$ nm as a function of the filed direction θ_H. The broken line is the calculated results derived from Stoner–Wohlfarth model, and the solid line is also the calculated one taking the experimentally determined c-axis dispersion $\Delta\theta_{50} \sim 6°$ into account [7].

with the Stoner–Wohlfarth (SW) model [14], in contrast with the $1/\cos\theta_H$ type behavior in Fig. 3 for larger FePt particles with $D \geqslant 60$ nm. The vertical axis in this figure is the normalized reversal field $h_r(\theta_H) = \eta H_r(\theta_H)/H_r(0)$, where η is the coefficient due to the c-axis dispersion. Rocking curve measurements gave the full width at half maximum of $\Delta\theta_{50} = 6°$ for our FePt particles, and this dispersion corresponds to $\eta = 0.82$. The dashed and solid lines in Fig. 10 indicate $H_r(\theta_H)$ for $\Delta\theta_{50} = 0°$ and 6°, respectively, calculated from the SW model. Note that the solid line is in very good agreement with the experiments. Therefore, it is concluded that the SW model (coherent rotation) is realized in this size region ($D \sim 10$ nm). On the other hand, for $d \geqslant 2$ nm ($D \geqslant 20$ nm), $h_r(\theta_H)$ becomes slightly asymmetric with respect to $\theta_H = 45°$, suggesting deviation from the SW model.

In order to investigate the magnetization reversal process in these FePt nanoparticles in more detail, the temperature dependence of H_c in Fig. 9 was analyzed by using the thermal fluctuation theory. Under the condition of easy axis//applied field H, El-Hilo et al. [15] derived the following formula based on the Néel–Brown model [12,16] as

$$H_c(T) = \eta H_k(T)\left\{1 - \sqrt{\frac{k_B T}{E_b(T)} \ln\left(\frac{k_B T H_k(T)}{2E_b(T)} \frac{f_0}{R}\right)}\right\}, \quad (3)$$

where R is the sweep rate of H. In the framework of the SW model, the anisotropy field H_k and the energy barrier E_b are represented as $2K_u/M_s$ and $K_u v$, respectively, where v is the particle volume. In this analysis, the temperature dependences of M_s and K_u, which have already been determined for FePt $L1_0$ (0 0 1) single crystal films [5], are taken into account. Moreover, the attempt factor f_0, which is usually used as a constant, is calculated from the formula given by Brown [17]. Therefore, all the parameters except for $H_k(0)$ and $E_b(0)$ are experimentally determined. The best fittings are given as the solid lines in Fig. 9, and all the experimental results can be reproduced very well. Thus determined $H_k(0)$ and $E_b(0)$ are plotted as a function of d in Fig. 11. $H_k(0)$ seems to be almost constant at 90 kOe, indicating that K_u remains very high even for smaller FePt particles with $D \sim 5$ nm and $h \sim 1$ nm. Using the value of $H_k(0)$, K_u can be evaluated as 6×10^7 erg/cc, which is comparable to the bulk value. On the other hand, $E_b(0)$ tends to increase with particle size. The broken line in Fig. 11 indicates the value of $K_u v$, where K_u is the value determined above and v is determined from the structural analysis. Note that $E_b(0)$ for $d < 2$ nm ($D < 20$ nm) coincides with $K_u v$ very well, indicating that the coherent rotation in this size region is dominant. On the other hand, $E_b(0)$ for $d \geqslant 2$ nm ($D \geqslant 20$ nm) clearly deviates from $K_u v$ and seems to be saturated. This deviation suggests the change in the reversal mode from coherent to incoherent rotation. Note that the values of $E_b(0)$ for $d \geqslant 2$ nm are comparable to that obtained in the lithographically fabricated single FePt particle as described in the previous section. From these results, we conclude that the size limit of coherent rotation in FePt nanoparticles exists around 20 nm. According to the micromagnetic theory of Aharoni [18], the critical size of coherent rotation of FePt for a thin oblate particle is evaluated as 38 nm, which is roughly consistent with the experimentally determined one.

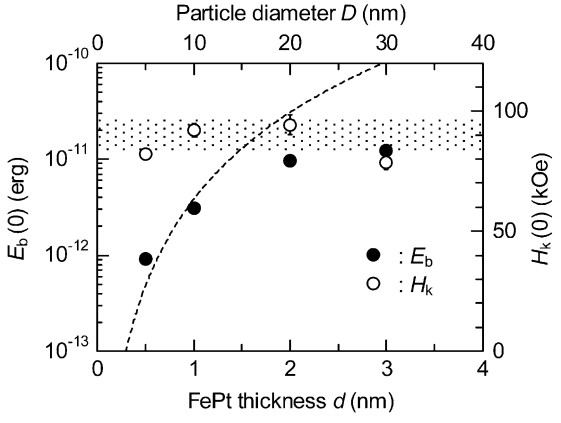


Fig. 11. Energy barrier $E_b(0)$ and anisotropy field $H_k(0)$ for epitaxially grown FePt $L1_0$ nanoparticle arrays determined from the best fitting in this figure as a function of nominal deposition thickness d. The broken line represents $K_u v$ [7].

4. Summary

We investigated size dependence of the magnetization reversal process for epitaxially grown FePt $L1_0$ (0 0 1) particles. For particle size $D = 60$–700 nm, the magnetization reversal in a lithographically fabricated single FePt particle was measured by anomalous Hall effect detection. A perfect bi-stable single domain state was found for $D < 80$ nm, although its reversals proceed by nucleation and subsequent expansion of a reversed embryo. Moreover, the temperature dependence of reversal mode could not be described by only one reversal mode, indicating co-existence of different reversal modes.

For smaller sizes of $D < 60$ nm, below the resolution limit of our e-beam lithography, epitaxially grown FePt $L1_0$ (0 0 1) nanoparticles were studied. For the particle size of $D < 20$ nm, all the magnetic behaviors, such as angular dependence of reversal field and temperature dependence of coercivity, were in good agreement with the behaviors calculated from the Stoner–Wohlfarth model and Néel–Brown model. Thus the critical size for coherent rotation in FePt nanoparticle was concluded as being around 20 nm, and this value is comparable to the expected one calculated from the micromagnetic theory.

The above results involve some of technological importance, and the findings in this study are valid not only for FePt $L1_0$ but also for other magnetic materials. When the particle is smaller than the critical size of coherent rotation, which can be roughly predicted by the micromagnetic theory, the recording performance and thermal stability of recorded signal can be simply described by the model based on the Stoner–Wohlfarth and Néel–Brown models. On the other hand, when the particle is larger than the above critical size, very complex incoherent reversal modes appear. Such complex modes hinder the stable operation of magnetic devices. Therefore, control of reversal modes will be very important in this size region.

Acknowledgments

The authors wish to thank Prof. K. Fukamichi of Tohoku University for operation of EB lithography, and Dr. Y.K. Takahashi and Dr. K. Hono of National Institute for Materials Science for TEM observations. This work has been supported by Industrial Technology Research Grant Program in 02 from NEDO of Japan, the Grant-in-Aid of the Japan Society for the Promotion of Science, the Special Coordination Funds for Promoting Science and Technology on "Nanohetero Metallic Materials" from the Ministry of Education, Culture, Sport, Science and Technology (MEXT), the IT-program RR2002 of MEXT, and the Storage Research Consortium in Japan.

References

[1] Mallary M, Torabi A, Benakli M. IEEE Trans Magn 2002;38:1719.
[2] Brown Jr WF. Rev Mod Phys 1945;17:15;
Aharoni A. Rev Mod Phys 1962;34:227.
[3] Givord D, Tenaud P, Viadieu T. IEEE Trans Magn 1988;24:1921.
[4] Livingston JD. IEEE Trans Magn 1987;MAG-23:2109.
[5] Okamoto S, Kikuchi N, Kitakami O, Miyazaki T, Shimada Y, Fukamichi K. Phys Rev B 2002;66:024413.
[6] Kikuchi N, Okamoto S, Kitakami O, Shimada Y, Fukamichi K. Appl Phys Lett 2003;82:4313.
[7] Okamoto S, Kikuchi N, Kitakami O, Shimada Y. Materia Jpn 2004;43:737.
[8] Okamoto S, Kitakami O, Kikuchi N, Miyazaki T, Shimada Y, Takahashi YK. Phys Rev B 2003;67:094422.
[9] Canedy CL, Gong GQ, Wang JQ, Xiao G. J Appl Phys 1996;79:6126.
[10] Thiele AA. J Appl Phys 1970;41:1139.
[11] Gaunt P. J Appl Phys 1986;59:4129.
[12] Néel L. Adv Phys 1955;4:191.
[13] Kikuchi N. PhD thesis, 2003.
[14] Stoner EC, Wohlfarth EP. Philos Trans R Soc Lond, Ser A 1948;240:599.
[15] El-Hilo M, de Witte AM, O' Grady K, Chantrell RW. J Magn Magn Mater 1992;117:L307.
[16] Brown WF. IEEE Trans Magn 1979;MAG-15:1196.
[17] Brown WF. J Appl Phys 1959;30:130S;
Brown WF. J Appl Phys 1963;34:1319.
[18] Aharoni A. J Appl Phys 1959;30S:70;
Aharoni A. Phys Stat Sol 1966;16:1.